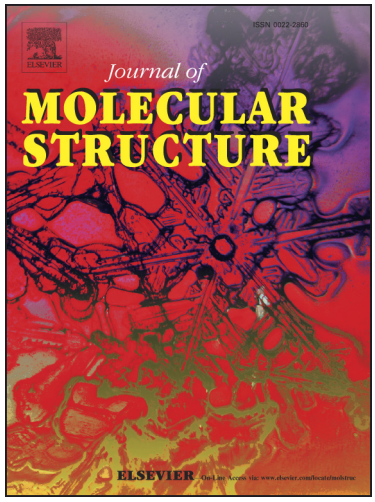

Spectroscopic and dynamic NMR study, X-ray crystallography and DFT calculations of two phosphoramidates: $(C_4H_3O_2)P(O)(Cl)C_6H_{14}N$ and $(C_4H_3O_2)P(O)(C_6H_{11}NH)_2$

F.M. Oliveira, L.C.A. Barbosa, A.J. Demuner, Célia R.A. Maltha, S.A. Fernandes, J.W.de M. Carneiro, R.S. Corrêa, A.C. Doriguetto

PII: S0022-2860(13)00379-7
DOI: http://dx.doi.org/10.1016/j.molstruc.2013.04.059
Reference: MOLSTR 19714

To appear in: *Journal of Molecular Structure*

Received Date: 27 February 2013
Revised Date: 22 April 2013
Accepted Date: 23 April 2013

Please cite this article as: F.M. Oliveira, L.C.A. Barbosa, A.J. Demuner, C.R.A. Maltha, S.A. Fernandes, J.M. Carneiro, R.S. Corrêa, A.C. Doriguetto, Spectroscopic and dynamic NMR study, X-ray crystallography and DFT calculations of two phosphoramidates: $(C_4H_3O_2)P(O)(Cl)C_6H_{14}N$ and $(C_4H_3O_2)P(O)(C_6H_{11}NH)_2$, *Journal of Molecular Structure* (2013), doi: http://dx.doi.org/10.1016/j.molstruc.2013.04.059

Spectroscopic and dynamic NMR study, X-ray crystallography and DFT calculations of two phosphoramidates: $(C_4H_3O_2)P(O)(Cl)C_6H_{14}N$ and $(C_4H_3O_2)P(O)(C_6H_{11}NH)_2$

F. M. Oliveira[a], L. C. A. Barbosa[a,b*], A. J. Demuner[a], Célia R. A. Maltha[a], S. A. Fernandes[a], J. W. de M. Carneiro[c*], R. S. Corrêa[d] and A. C. Doriguetto[e]

[a] *Chemistry Department, Federal University of Viçosa, CEP 36570-000, Viçosa, MG, Brazil*

[b] *Chemistry Department, Federal University of Minas Gerais, CEP 34095-720, Belo Horizonte, MG, Brazil*

[c] *Inorganic Chemistry Department, Fluminense Federal University, CEP 24020-141, Niterói, RJ, Brazil*

[d] *São Carlos Physics Institute – USP, Cx. postal 369, CEP 13560-970, São Carlos, SP, Brazil*

[e] *Institute of Chemistry, Federal University of Alfenas, CEP 37130-000, Alfenas, MG, Brazil*

[*] Corresponding authors. (L.C.A.B)Tel.: +55 313899 3068; e-mail: lcab@ufmg.br; (J.W.M.C) Tel.: +55 21 26295114; e-mail: walk@vm.uff.br

Abstract - In recent years, research in organophosphorus compounds, particularly phosphoramidates, has attracted attention because of their many applications. In this work, we report a combined experimental and theoretical study on the molecular structure and NMR spectra of two phosphoramidates (furan-2-yl *N,N*-diisopropylamidochlorophosphate (**1**) and furan-2-yl *N,N,N′,N′*-dicyclohexylamidophosphate (**2**)). In the NMR time scale a free rotation of the C-N/P-N single bonds was observed at room temperature (298 K) while the rotation freezes below 195 K for compound **1**. From dynamic NMR analysis, the activation free energy ($\Delta G^{\#}$) for rotation of the C-N/P-N bonds was calculated as 9.9 ± 0.3 kcal mol^{-1}. The experimental data were reinforced by theoretical calculation using the density functional theory method B3LYP and the 6-31G(d) basis set which provided activation energy ($\Delta E^{\neq}$) of 9.2 kcal mol^{-1}. The structures of compounds **1** and **2** were determined by single crystal X-ray diffraction method. Compound **1** is formed by a racemic mixture, whose presence was evidenced only in the structure determination by X-ray.

Keywords: Phosphoramidate; Crystal structure; Coalescence energy; DFT calculations; Insecticides, Dynamic NMR.

1. Introduction

Organophosphorus compounds have attracted great attention due to their biological activities. Among these, one of the most common class are the phosphoramidates, which are characterized by the presence of at least one $–NR^1R^2$ group (R^1 and R^2 = alkyl, aryl) in their structures. Phosphoramidates are extensively studied due to their potential applications as acetylcholinesterase and urease inhibitors [1], insecticides [2,3], herbicides [4], antifire [5], anticancer drugs [6-8], anti HIV [9-10], inhibitors of hepatitis C virus [11-12], antimalarial agents [13], and antirust additives in lubricating oils [14]. Moreover, novel synthesized phosphoramidate derivatives of fenoprofen, ketoprofen, ibuprofen, indomethacine and diclofenac possess significantly higher antiproliferative activities than the corresponding nonsteroidal anti-inflammatory drugs (NSAID) 3-hydroxypropylamides [15].

Continuing our effort to develop new compounds with insecticidal [2,3] and phytotoxic activity [16-19], we have synthesized new phosphoramidates and quantified their activity against the Lepidoptera species that attack important commercial crops [3]. Among the synthesized compounds, only furan-2-yl *N,N*-diisopropylamidochlorophosphate (**1**) and furan-2-yl *N,N,N′,N′*-dicyclohexylamidophosphate (**2**) were obtained as single crystals (Fig. 1).

Insert Figure 1

The biological functions of the phosphoramidates most probably are correlated to their molecular properties [20-23]. Although the crystal structures of some phosphoramidates have been reported recently [24-27], only a few details about the structural and spectral properties of such substances have been described in the literature. Knowledge of structure and molecular properties are important for the detailed

understanding of their effect on the biological functions and help the rational design of new compounds [28].

Our aim is to provide valid support to the structural characterization of the phosphoramidates. Dynamic NMR studies have been extensively used to explore the kinetics and thermodynamics of stereo dynamic processes [29]. Thus, we report the dynamic ^{1}H and ^{13}C NMR spectra and use them to estimate the rotational barrier activation free energy ($\Delta G^{\ddagger}$) for hindered rotation of the C-N and P-N bonds [30] in phosphoramidate **1**. Additionally, the single crystal X-ray diffraction data and quantum chemical calculations using Density Functional Theory (DFT) are also reported.

2. Experimental

2.1. NMR Studies

One dimensional ^{1}H- and ^{13}C-NMR spectra were acquired either with an MERCURY-300/Varian spectrometer at 300.069 MHz for ^{1}H (32 k data points, 30^{o} excitation pulse duration of 2.2 μs, spectral width of 6 KHz, acquisition time of 3.3 s and relaxation delay of 10 ms) and at 75.452 MHz for ^{13}C (32 K data points 45^{o} excitation pulse duration of 6.5 μs, spectral width of 19 KHz, acquisition time of 0.8 s and relaxation delay of 2.0 s) in 5 mm probes with direct detection, using deuterated dichloromethane or chloroform as a solvent and TMS as internal standard (δ = 0.00).

2.2 - Single-crystal X-ray diffraction

Crystals of compounds **1** and **2** were obtained by gently warming each compound in hexane, followed by addition of dichloromethane dropwise until the solid was completely dissolved. The resulting solution was left undisturbed at room temperature. After 24 hours, white crystals, suitable for X-ray analyses, were formed. They were separated, washed with cold hexane, and dried.

Well-shaped single crystals of **1** and **2** were chosen for the X-ray experiment. The measurements were made at 298 K on an Enraf-Nonius Kappa-CCD difractometer with graphite monochromated Mo Kα. Data were collected up to ~50° in 2θ, with a redundancy of 4. The final unit cell parameters were based on all reflections. The temperature was controlled using an Oxford Cryosystem low temperature device. Data collection was made using the *COLLECT* software [31]; integration and scaling of the reflections were performed with the HKL Denzo-Scalepack software system [32]. The structures were solved and the models refined using the SHELXL-97 software [33]. H atoms on C atoms were positioned stereochemically and were refined with fixed individual displacement parameters [$U_{iso}(H) = 1.5U_{eq}(C)$ for methyl groups or $1.2U_{eq}(C)$ for aromatic, methine and methylene groups], using the SHELXL riding model with C—H bond lengths of 0.96, 0.98 and 0.97 Å for methyl, methine and methylene groups, respectively. The hydrogen atoms bonded to the nitrogen atoms in **2** were found in successive difference Fourier maps and were refined with free coordinates and $U_{iso}(H) = 1.2U_{eq}(O)$. WINGX software was used to analyze and prepare the data for publication. Molecular graphics were prepared using ORTEP-3 for Windows [34] and Mercury [35]. Crystal data, data collection procedures, structure determination methods and refinement results are summarized below.

2.3. Computational Details

The geometries of the two phosphoramidates **1** and **2** were first designed in the SPARTAN´10 software [36]. Using the conformer distribution routine of SPARTAN and the semi-empirical PM3 method [37] a conformational analysis of both species was carried out to identify the most stable conformers in each case. Those conformers were then reoptimized with the B3LYP functional [38,39] and the 6-311++G(2d,p) basis set. Approximated activation energies for rotation around either the P-N or the C-N bonds were obtained by a relaxed dihedral scan (by 30º step) around the corresponding bond using the 6-31G(d) basis set. All the DFT calculations were performed using the Gaussian 09 program package [40].

3. Results and discussion

In a previous work we have described the preparation of some lactone analogous to the natural compounds called nostoclides [17]. Lactone **3**, used as starting material, was synthesized previously [2]. The treatment of **3** with $POCl_3$ in the presence of triethylamine afforded compound **4** (Scheme 1), which was not isolated. Subsequent reaction of **4** with diisopropylamine (2 eq.) and DMAP (5 mol%) furnished **1** in 14% yield. Formation of **1** resulted from substitution of one of the chlorine atoms in **4** by the diisopropylamino group. Treatment of **4** with cyclohexylamine (2 eq.) and DMAP (5 mol%) furnished **2** in 10% yield, with the complete substitution of chlorine atoms in **4** by the nucleophilic cyclohexylamine [3]. The products were obtained as white crystals and the structures of compounds **1** and **2** were confirmed by single crystal X-ray diffraction (Figs. 2 and 6).

Insert Scheme 1

Crystal structure analysis

Crystal data, data collection procedures, structure determination methods and refinement results are summarized in Table 1. Crystallographic data for the structural analysis of the compounds discussed here have been deposited at the Cambridge Crystallographic Data Centre, 12 Union Road, Cambridge CB2 1EZ, UK, and are available on request quoting the deposition numbers CCDC 902881 and 902882, for **1** and **2**, respectively.

Insert Table 1

Figure 2 shows the *R* enantiomer of **1**. Table 2 gives selected experimental and calculated bond length and angles. Since **1** is a chiral molecule crystallized in a centrosymmetric space group, its crystal structure is formed by an equimolar mixture of a pair of enantiomers (*R/S*: 50/50) (Fig. 3). The intermolecular geometry of **1** was analyzed using Mogul [41], a knowledge base of molecular geometry derived from the Cambridge Structural Database (CSD; Version 5.33 of November 2011, with January 2012 and May 2012 updates) [42]. This analysis shows that all bond lengths and bond angles are in agreement with the values expected for a good X-ray diffraction structure refinement. The extended least-squares plane through the furan ring including the exocyclic atom O2

[r.m.s = 0.0024 Å and largest deviation = 0.003(2) Å for O3], shows that this moiety is planar, as expected.

Insert Table 2

Insert Figure 2

Insert Figure 3

The intermolecular analysis of **1** shows that a non-classical hydrogen bond [C—H = 0.93 Å, C…O = 3.364(3) Å, H4…O = 2.502(3) Å, C—H…O = 154.26^{o}] involving the furan and P=O group is the main intermolecular force that contributes to the stabilization of the crystal packing (Figs. 4 and 5). The individual chains are themselves linked by VDW interactions forming a racemic double chain along [010]. The furan rings in the double chains are laid in plane parallel to (101) forming a ribbon along [010] (Figs. 4 and 5). The shortest Cl…Cl separation is 5.581(3) Å, which is slightly longer than the limit (3.52 Å) to be considered as an intermolecular halogen-halogen interaction involving chlorine [43].

Insert Figure 4

Insert Figure 5

Figure 6 shows an ORTEP view of **2** with the ring label scheme. The main geometric parameters are given in Table 1 and some experimental and calculated bond length and bond angles are given in Table 3. Similarly to compound **1**, the molecular conformation of **2** was also analyzed using the MOGUL software, which revealed a good X-ray diffraction refinement. The extended least-squares plane through the furan ring including the exocyclic O2 atom [r.m.s = 0.0206 Å and largest deviation = -0.029(1) Å for O2] shows that also in this case this moiety is considerably planar. The intermolecular arrangement of the furan rings in **1** and **2** shows that they are similar, as expected. However, their orientations are different in relation to the O1=P1-O2 plane in the phosphorus tetrahedral moiety (Fig. 7). The least-squares plane through the furan ring and the O1=P1-O2 triad form angles of 73.97(7)^{o} and 53.6(1)^{o} for **1** and **2**, respectively. Moreover, in **1** the P=O bond is oriented *anti* to the C1—O3 bond, whereas in **2** the corresponding arrangement is *syn* (Fig. 7). Both cyclohexyl moieties have chair conformation with weighted average absolute torsion angles of 54.87(10.52)° and 55.42(12.23)° for rings B and C, respectively (1st is the e.s.d. internal and 2nd is the

external one) [44]. Considering the two possible chair conformations of the cyclohexylamine ring, the C5—N1 and C11—N2 bonds are both in equatorial orientation.

Insert Figure 6

Either the N1—H1 or N2—H2b groups act as intermolecular H bond donor to the O1, giving rise to an infinite one-dimensional chain parallel to the [010] direction (Fig. 8 and Table 4). The linkage takes place through the phosphorous tetrahedron by glide b (normal to *a* axis)- and translation-related molecules. The orientation of individual chains along [010] is shown in the packing illustration of **2** onto the plane ac (Fig 9).

Insert Table 3

Insert Figure 7

Insert Figure 8

Insert Figure 9

Insert Table 4

NMR study

The ^{1}H- and ^{13}C-NMR spectra at 298K evidence couplings over long distances in both phosphoramidates, **1** and **2**. The ^{1}H-NMR spectra of compounds **1** and **2** show three double double doublets corresponding to H-3, H-4 and H-5 (Fig. 10). The furan hydrogen couples with neighboring hydrogen atoms and shows a ddd splitting pattern due to its coupling with phosphorus atom at 4 to 5 bond distance (Fig. 10). The *J* values at 298 K are shown in Table 5. The NMR spectrum of compound **2** also shows a multiplet at δ 3.03-3.18 for the –CH group coupled with the H_{ax} and H_{eq}. A multiplet integrated for 20 hydrogen atoms at δ 1.05-1.96 for the hydrogen atoms of cyclohexyl coupled with neighboring hydrogen atoms was also observed. For the NH signal of compound **2** a two bond distance coupling with the P atom and a two bond distance coupling with –CH of cyclohexyl were observed. A triplet signal at δ 2.64 is obtained for NH with $^{2}J_{P,NH} \approx {}^{2}J_{NH,CH} \approx 10$ Hz, a value similar to that described in the literature [25]. The ^{1}H NMR spectrum of **1** displays two doublets at δ 1.29 and 1.34 integrated for 6 hydrogen atoms each ($^{2}J_{CH3,CH} = 6.9$ Hz) for the two types of CH_3 groups of the isopropyl moieties due to the fact that the carbon atom of the CH group in the isopropyl substituent is prochiral.

The methine hydrogen of the isopropyl groups appears as a double septet at δ 3.63 and 3.69 integrated for 2 hydrogen atoms ($^3J_{P,\ CH}$ = 24.3 Hz) due to its coupling with the methyl groups and the phosphorus atom. This analysis indicates that the rotational energy barrier around the C-N and P-N bonds must be low, consistent with the equivalent chemical shifts shown by the isopropyl moieties on the NMR timescale.

Insert Figure 10

The ^{13}C NMR spectra of compounds **1** and **2** show three doublets (δ 89, 111 and 135, respectively) due to carbon atoms C-3, C-4 and C-5 (Fig. 11). The signal multiplicities are due to carbon coupling with phosphorus atom at a distance of 3-4 bonds. Curiously, lower $J_{P,C}$ were obtained for compound **2** (Table 5) than for compound **1**. The quaternary carbon atoms of compounds **1** and **2**, C-2 (Fig. 11), are coupled to phosphorus at δ 149-152 ($^2J_{P,C}$ = 6.5 and 5.1 Hz, respectively). For both compounds couplings at long distances were observed, but $^2J_{P,CH}$ coupling was not observed for compound **2**. A similar behavior was observed for the phosphoramidates described by Souza et al. (2006) [45]. The ^{13}C spectrum of compound **1** shows distinct signals for the diastereotopic methyl carbon atoms which appeared as doublets ($^3J_{CH3,P}$ = 2.5 and 1.6 Hz) due to $^3J_{PNC}$ coupling, whereas the methine carbon atom doublet shows larger $^2J_{PNC}$ coupling ($^2J_{CH,P}$ = 4.9 Hz). The ^{13}C NMR spectrum of compound **2** exhibits three signals for the ten carbon atoms of the –CH_2 cyclohexyl moieties. These results indicate that the spatial orientations of the aliphatic six-membered rings are the same. A ($^3J_{P,CH2}$) coupling constant of 5.4 Hz was observed for the splitting of the -CH_2 carbon atom with the phosphorus atom. The spectrum observed in this experiment for compound **1** was found to correspond to that of a racemic mixture, whose evidence appeared only in structure determination by X-ray (Fig. 3).

Insert Figure 11

Insert Table 5

An important point in the discussion of the equilibrium geometries of the phosphoramidates is the activation barrier for rotation around the C-N and P-N bonds. From the analysis of a molecular model, a 180º rotation around the P-N bond, followed by a 180º rotation around each C-N bonds, results in the equivalence of the two isopropyl groups. With this in mind, we carried out a NMR variable temperature study for

compound **1**. The results allowed calculation of the higher free energy barrier for rotation, but would not allow us to know which bond (C-N or P-N) corresponds to the experimental data. From the temperature of coalescence of the hydrogen lines the first-order rate constant ($k_{coalescence}$) was calculated from the expression $k_{coalescence} = \pi(\Delta\nu^2 + 6J^2)^{1/2}/(2^{1/2})$ where $\Delta\nu$ is the difference in chemical shift between the centers of the two doublets arising from the methyl hydrogen atoms, and J is the coupling constant. From the ^{13}C NMR and the coalescence temperature, the rate constant is related to the chemical shift difference from the expression $k_{coalescence} = \pi(\Delta\nu)/(2^{1/2})$ where $\Delta\nu$ is the difference in chemical shift. Substituting this value into the Eyring rate equation gives the expression $\Delta G^{\ddagger} = RT\ln(6.62x10^{12}/k_{coalescence})$ [46]. For comparison, the value of the free energy barrier was calculated from the coalescence of the resonances and by theoretical methods.

The behavior of **1** was monitored by ^{1}H-NMR techniques at variable temperatures. From the data, the relevant thermodynamic parameters were calculated. To examine their behavior, the NMR tube containing compound **1** was placed in the NMR probe and cold slowly from 298 K to 178 K.

The determination of the exact temperature inside the sample is crucial for the determination of the thermodynamic parameters. An error of ± 2 °C in the temperature causes an error in $\Delta G^{\#}$ of 0.15 to 0.2 kcal mol^{-1} and this is usually the main source of errors in the dynamic NMR technique [47]. Therefore, the coalescence temperature was determined by performing several ^{1}H NMR experiments (Figs. 12 and 13).

Insert Figure 12

Insert Figure 13

For compound **1**, two separate doublets appeared in the ^{1}H-NMR spectrum at 298 K for the methyl carbons of the isopropyl groups since they are diastereotopic. In this condition there is a free rotation of the C-N and P-N single bonds so that the isopropyl groups become equivalent. Also, in the ^{13}C NMR spectrum of **1** at this temperature, two signals (Fig. 13: a = c ≠ b = d and Scheme 2) are observed for the methyl carbons of the isopropyl groups. At low-temperature (< 195K), ^{1}H and ^{13}C NMR spectra of compound **1** show signals for two diastereotopic isopropyl groups. Therefore, four signals are observed for the methyl carbons (Fig. 13: a ≠ c ≠ b ≠ d and Scheme 2) and two signals for –CH (Fig. 13: e ≠ f and Scheme 2).

Insert Scheme 2

The collected ^{1}H NMR spectra relevant to the dynamic effect are shown in the following variable-temperature NMR (Figs. 12 and 13).

The coalescence temperature was eventually observed at T_C = 195 K in ^{1}H NMR, and the higher activation energy ($\Delta G^{\#}$) for rotation around the C-N and P-N single bonds was calculated as 9.9 ± 0.3 kcal mol^{-1}. From this experiment we cannot attribute the calculated value to $\Delta G^{\#}$ for rotation of C-N or P-N bonds. So, in order to better understand this process, a molecular computational analysis was carried out.

Computational analysis

To help rationalize the experimental findings, we carried out a set of calculations for phosphoramidates **1** and **2**. The most stable conformers of **1** and **2** were obtained using the semi-empirical PM3 method [37] in the Spartan software. The geometry of that conformations were then reoptimized using the B3LYP/6-311++G(2d,p) approach. Each optimized geometry was confirmed as a local minimum on the potential energy surface. Selected parameters of the most stable optimized geometries are compared with the X-ray diffraction data in Tables 2 and 3, which show that in general the experimental and computed parameters are in close agreement. The only cases that deserve some attention are the bond angles O1-P1-O2, C8-N1-C5 in **1** and O2-P1-N2 in **2**. The computed values for the O1–P1–O2 bond angles for compounds **1** and **2** are 115.70 and 116.18(°), respectively. The corresponding experimental bond angles are 110(4)(°) and 113(2)(°). For the C8–N1–C5 bond angle in **1** the difference between the experimental and theoretical values is a bit larger, amounting to 6.9°. For the O2-P1-N2 bond angle in **2** the corresponding difference is 5.7°.

In addition to the determination of the most stable geometry for each phosphoramidate we also calculated the approximated activation energy for rotation around the P-N and C-N single bonds for **1**. The goal was to identify whether the activation parameters determined in the dynamic NMR studies are consistent with activation energies for rotation around these bonds.

The dynamic process represented in Scheme 2 is enough to interconvert the pairs of diastereotopic isopropyl groups, however, to completely equilibrate the four methyl

groups (a, b, c and d in Scheme 2) we have also to consider rotation around the C-N bonds. To determine the activation parameter in each case we performed a set of calculations with the dihedral angle involving both the P-N and the C-N bonds fixed at a given value and optimization of the additional degree of freedom. Starting from 0^o the dihedral angle was increased by a 30^o step in each case up to the value of 330^o. With this, we could not only confirm the structure of minimal energy but also determine the transition structure for rotation around the corresponding bond. The B3LYP/6-31G(d) approach was employed for these calculations.

Rotation around the P-N bond revealed two minima, the global minimum energy structure, with one of the C-N bonds eclipsing the phosphoryl P=O bond and a local minimum energy structure with the lone pair on the nitrogen atom eclipsing the P-Cl bond, 2.1 kcal.mol^{-1} less stable than the global minimum. The activation energy for interconversion between these two minima is 6.8 kcal mol^{-1} (TS1). On the other hand, rotation around each of the C-N bond also revealed two minima, the global minimum energy structure and a second one, 3.3 kcal mol^{-1} above the global minimum. The activation barrier for rotation around the C-N bond is 9.2 kcal mol^{-1} (TS2). The last value closely fits the experimental 9.9±0.3 kcal mol^{-1} obtained by dynamic NMR studies. Based on these results we are suggesting that the dynamic behaviour in these phosphoramidates is characterized by rotation around both the P-N and the C-N bonds, with activation energy for rotation around the C-N bonds being the higher value. According to Scheme 2 rotation around the P-N bond interchanges the isopropyl groups but not the methyl groups within each isopropyl groups. Complete equilibration of the methyl groups occurs only after rotation around the C-N bond, which is the process with the higher activation energy.

4. Conclusion

In an effort to prepare new compounds with potential biological activity and rationalize their molecular properties, two phosphoramidates have been studied by dynamic NMR, theoretical calculation, spectroscopic data and X-ray crystallography. Compound **1** is a chiral molecule crystallized in a centrosymmetric space group as an

equimolar mixture of a pair of enantiomers (*R/S*: 50/50). Geometrical parameters calculated with DFT methods are consistent with the experimental X-ray data. The dynamic behavior of **1** was investigated by NMR spectroscopy, which revealed the activation energy of 9.9 ± 0.3 kcal mol^{-1}. Based on computational calculation of the activation energies for rotation around the P-N and C-N bonds, this experimental value was attributed to the C-N bond.

Acknowledgments

We thank Conselho Nacional de Desenvolvimento Científico e Tecnológico (CNPq), Fundação de Amparo à Pesquisa do Estado de Minas Gerais (FAPEMIG) and Fundação Arthur Bernardes (FUNARBE) for financial support and research fellowships (ACF, AJD, JWMC, ACD, LCAB,SAF and FMO). We thank Prof. Javier Ellena for support during the single-crystal diffraction measurements.

References

[1] M.J. Dominguez, C. Sanmartin, M. Font, J.A. Palop, S.S. Francisco, O. Urrutia, F.Houdusse, J.M. Garcia-Mina, J. Agric. Food Chem., 56 (2008) 3721-3731.

[2] V.F. Paula, L.C.A. Barbosa, R.R. Teixeira, M.C. Picanço, G.A. Silva, Pest Manag. Sci., 64 (2008) 863-872.

[3] F.M. Oliveira, L.C.A. Barbosa, R.R. Teixeira, A.J. Demuner, C.R.A. Maltha, M.C. Picanço, G.A. Silva, V.F. Paula, J. Pestic Sci., 37 (2012) 85-88.

[4] T. Katagi, J. Agric. Food Chem., 41 (1999) 496-501.

[5] Y.B. Kiran, C.D. Reddy, D. Gunasekar, C.N. Raju, L.C.A. Barbosa, D.C.O. Marney, L.J. Russell, J. Fire Sci., 25 (2007) 193-215.

[6] Y.B. Kiran, C.D. Reddy, D. Gunasekar, C.S. Reddy, A. Leon, L.C.A. Barbosa, Eur. J. Med. Chem., 43 (2008) 885-892.

[7] D.I. Niculescu, I. Scanlon, D. Niculescu, F. Friedlos, J. Martin, R. Marais, C.J. Springer, J. Med. Chem., 47 (2004) 2651-2658.

[8] Z. Wang, C. Guo, W. Xie, C. Liu, C. Xiao, Z. Tan, Eur. J. Med. Chem., 45 (2010) 890-895.

[9] Y. Mehellou, J. Balzarini, C. McGuigan, Org. Biomol. Chem., 7 (2009) 2548-2553.

[10] I. Zlatev, A. Giraut, F. Morvan, P. Herdewijn, J. Vasseur, Bioorg. Med. Chem., 17 (2009) 7008-7014.

[11] C. McGuigan, M.R. Kelleher, P. Perrone, S. Mulready, G. Luoni, F. Daverio, S. Rajyaguru, S.L. Pogam, I. Najera, J.A. Martin, K. Klumpp, D.B. Smith, Bioorg. Med. Chem. Lett., 19 (2009) 4250-4254.

[12] M. Donghi, B. Attenni, C. Gardelli, A.D. Marco, F. Fiore, C. Giuliano, R. Laufer, J.F. Leone, V. Pucci, M. Rowley, F. Narjes, Bioorg. Med. Chem. Lett., 19 (2009) 1392-1395.

[13] C. Mara, E. Dempsey, A. Bell, J.W. Barlow, Bioorg. Med. Chem. Lett., 21 (2011) 6180-6183.

[14] J. Yan, J. Bu, X. Bai, J. Li, T. Ren, Y. Zhao, J. Engineering Tribology, 226 (2012) 377-388.

[15] K. Wittine, K. Benci, Z. Rajic, B. Zorc, M. Kralj, M. Marjanovic, K. Pavelic, E. De Clercq, G. Andrei, R. Snoeck, J. Balzarini, M. Mintas, Eur. J. Med. Chem., 44 (2009) 143-151.

[16] L.C.A. Barbosa, C.R.A. Maltha, A.J. Demuner, F.R. Ganen, A.A. Silva, Quim. Nova, 28 (2005) 444-450.

[17] L.C.A. Barbosa, A.J. Demuner, E.S. Alvarenga, A. Oliveira, B. King-Diaz, B. Lotina-Hennsen, Pest Manag. Sci., 62 (2006) 214-222.

[18] L.C.A. Barbosa, U.A. Pereira, R.R. Teixeira, C.R.A. Maltha, S.A. Fernandes, G. Forlani, J. Agric. Food Chem., 56 (2008) 9434-9440.

[19] L.C.A. Barbosa, C.R.A. Maltha, R.C. Cusati, R.R. Teixeira, F.F. Rodrigues, A. A. Silva, M.G.B. Drew, F.M.D. Ismail, J. Agric. Food Chem., 57 (2009) 10107-10115.

[20] R.S. Corrêa, S.R. Souza e Silva, L.P. Duarte, G.D.F. Silva, L.C.A. Barbosa, J. Ellena, A.C. Doriguetto, J. Struct. Chem., 53 (2012) 156-163.

[21] R.R. Teixeira, L.C.A. Barbosa, J.W.M. Carneiro, R.S. Corrêa, J. Ellena, A.C. Doriguetto, J. Mol. Struct., 917 (2009) 1–9.

[22] F.T. Martins, I. Campsa, A.C. Doriguetto, M.H. dos Santos, J. Ellena, L.C.A. Barbosa, Helv. Chim. Acta, 91 (2008) 1313-1324.

[23] R.R. Teixeira, L.C.A. Barbosa, J.O. Santana, D.P. Veloso, J. Ellena, A.C. Doriguetto, M.G.B. Drew, F.M.D. Ismail, J. Mol. Struct., 837 (2007) 197-205.

[24] K. Gholivand, C.O.D. Védova, M.F. Erben, H.R Mahzouni, Z. Shariatinia, S. Amiri, J. Mol. Struct., 874 (2008) 178-186.

[25] K. Gholivand, M. Pourayoubi, Z. Shariatinia, H. Mostaanzadeh, Polyhedron, 24 (2005) 655-662.

[26] K. Gholivand, H. Mostaanzadeh, T. Koval, M. Dusek, M.F. Erben, H. Stoeckli-Evans, C.O.D. Védova, Acta Cryst., B66 (2010) 441-450.

[27] K. Gholivand, F. Afshar, Z. Shariatinia, K. Zare, Struct. Chem., 21 (2010) 629-636.

[28] S. Dehghanpour, R. Welter, A.H. Barry, F. Tabasi, Spectrochim. Acta Part A, 75 (2010) 1236-1243.

[29] T.G. Peck, Y.H. Lai, Tetrahedron, 65 (2009) 3664-3667.

[30] K. Marjani, M. Mousavi, H.T. Nahzomic, O. Arazi, R. Jafari, Spectrochim. Acta Part A, 79 (2011) 1798-1802.

[31] Nonius, COLLECT. Nonius BV, Delft, The Netherlands, 1999.

[32] Z. Otwinowski, and W. Minor, Methods in Enzymology, (1997) Vol. 276, Macromolecular Crystallography, Part A, edited by C. W. Carter Jr & R. M. Sweet, pp. 307–326. New York: Academic Press.

[33] G.M. Sheldrick, Acta Cryst., A64 (2008) 112–122.

[34] L.J. Farrugia, J. Appl. Cryst., 30 (1997) 565.

[35] C.F. Macrae, P.R. Edgington, P. McCabe, E. Pidcock, G.P. Shields, R. Taylor, M. Towler, and J. van de Streek, J. Appl. Cryst., 39 (2006) 453–457.

[36] Spartan ’10, Wavefunction Inc., Irvine, CA, USA.

[37] J.J.P.J. Stewart, Comput. Chem., 10 (1989) 221-264

[38] A.D. Becke, Phys. Rev. A, 38 (1988) 3098-3100.

[39] C. Lee, W. Yang, R.G. Parr, Phys. Rev. B, 37 (1988) 785-789.

[40] M.J. Frisch, G.W. Trucks, H.B. Schlegel, G.E. Scuseria, M.A. Robb, J.R. heeseman, G. Scalmani, V. Barone, B. Mennucci, G.A. Petersson, H. Nakatsuji, M.

Caricato, X. Li, H.P. Hratchian, A.F. Izmaylov, J. Bloino, G. Zheng, J.L. Sonnenberg, M. Hada, M. Ehara, K. Toyota, R. Fukuda, J. Hasegawa, M. Ishida, T. Nakajima, Y. Honda, O. Kitao, H. Nakai, T. Vreven, J.A. Montgomery, Jr., J.E. Peralta, F. Ogliaro, M. Bearpark, J.J. Heyd, E. Brothers, K.N. Kudin, V.N. Staroverov, R. Kobayashi, J. Normand, K. Raghavachari, A. Rendell, J.C. Burant, S.S. Iyengar, J. Tomasi, M. Cossi, N. Rega, J.M. Millam, M. Klene, J.E. Knox, J.B. Cross, V. Bakken, C. Adamo, J. Jaramillo, R. Gomperts, R.E. Stratmann, O. Yazyev, A.J. Austin, R. Cammi, C. Pomelli, J.W. Ochterski, R.L. Martin, K. Morokuma, V.G. Zakrzewski, G.A. Voth, P. Salvador, J.J. Dannenberg, S. Dapprich, A.D. Daniels, Ö. Farkas, J.B. Foresman, J.V. Ortiz, J. Cioslowski, D.J. Fox, Gaussian 09, Revision A1, Gaussian Inc., Wallingford CT, 2009.

[41] I.J. Bruno, J.C. Cole, M. Kessler, J. Luo, W.D.S. Motherwell, L.H. Purkis, B.R. Smith, R. Taylor, R.I. Cooper, S.E. Harris, and A.G. Orpen, J. Chem. Inf. Comput. Sci., 44 (2004) 2133–2144.

[42] F.H. Allen, Acta Cryst., B58 (2002) 380–388.

[43] G.R. Desiraju, and R. Parthasarathy, J. Am. Chem., 111 (1989) 8725-8726.

[44] A. Domenicano, A. Vaciago, and C.A. Coulson, Acta Cryst., B31 (1975) 221-234.

[45] M.C. de Souza, W.P. de Macedo, T.S. Torres, L.F. Pedrosa, H.G. Alt, Phosphorus, Sulfur, and Silicon and the Related Elements, 181 (2006) 1885-1893.

[46] E. Breitmaier, W. Voelter, ^{13}C NMR Spectroscopy, 3nd ed., Verlag Chemie, Weinheim, New York, 1987.

[47] B.F. Bonini, L. Grossi, L. Lunazzi, D. Macciantelli, J. Org. Chem., 51 (1986) 517-522.

Highlights

- In the NMR time scale a rotation of the C-N and P-N single bonds froze at 195 K.
- $\Delta G^{\#}$ for rotation of the C-N bond of phosphoramidates was calculated by dynamic NMR
- Compound **1** crystallized in a centresymmetric space group as a mixture of enantiomers
- Geometrical parameters obtained by DFT are consistent with experimental X-ray data

Captions for the ilustrations

Scheme1.

Synthesis of phosphoramidates **1** and **2** described by Oliveira and co-workers (2012).

Scheme 2.

Interchangeable processes of compound **1** at 298K.

Fig. 1.

Structure of compounds **1** and **2**.

Fig. 2.

The molecular structure of **1** (*R* enantiomer), showing the atom numbering scheme. Displacement ellipsoids are drawn at the 30% probability level and H atoms are shown as small spheres of arbitrary radii.

Fig. 3.

Molecular fragments highlighting the two enantiomers, a) *R* (molecule in x, y, z) and b) *S* (molecule in -x, -y, -z).

Fig. 4.

A partial packing diagram for **1**, showing the racemic double chain formed along [010]. Hydrogen bonds are shown as dashed lines. [Symmetry codes: (i) x, y-1, z; (ii) x, y+1, z; (iii) -x+1, -y+1, -z+1; (iv) -x+1, -y+2, -z+1].

Fig. 5.

The crystal packing illustration of **1** onto the plane ac. Hydrogen atoms were omitted for clarity.

Fig. 6.

The molecular structure of **2** with atom and ring labeling. Displacement ellipsoids are drawn at the 30% probability level and H atoms are shown as small spheres of arbitrary radii.

Fig. 7.

Relative orientation of the furan ring and phosphorus tetrahedron in (a) **1** and (b) **2**.

Fig. 8.

(a) View of the network of hydrogen bonds parallel to [001] which stabilizes the packing of **2**. (b) View showing only the phosphorous tetrahedral and atom labeling involved in the hydrogen bonds. Symmetry codes: $^{(i)}$ = *-x-1/2, y+1/2, z;* $^{(ii)}$ = *x, y+1, z;* $^{(iii)}$ *-x-1/2, y-1/2, z.*

Fig. 9.

Packing illustration of **2** onto the plane ac. Hydrogen atoms were omitted for clarity. The colors represent the eight equivalent positions of Pbac space group.

Fig. 10.

The ^{1}H NMR spectra of compounds **1** and **2** at 298 K in $CDCl_3$.

Fig. 11.

The ^{13}C NMR spectra of the compounds **1** and **2** at 298 K in $CDCl_3$.

Fig. 12.

The variable temperature ^{1}H NMR spectra of **1** from 298 to 178 K in CD_2Cl_2.

Fig. 13.

The variable temperature ^{13}C NMR spectra of **1** from 298 to 193 K in CD_2Cl_2.

Fig. 1.

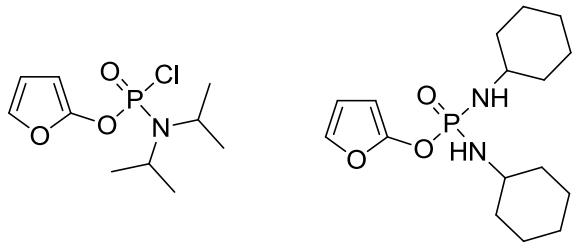

1 **2**

Fig. 2.

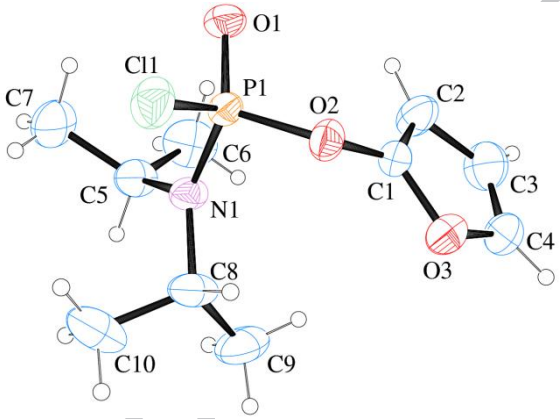

Fig. 3.

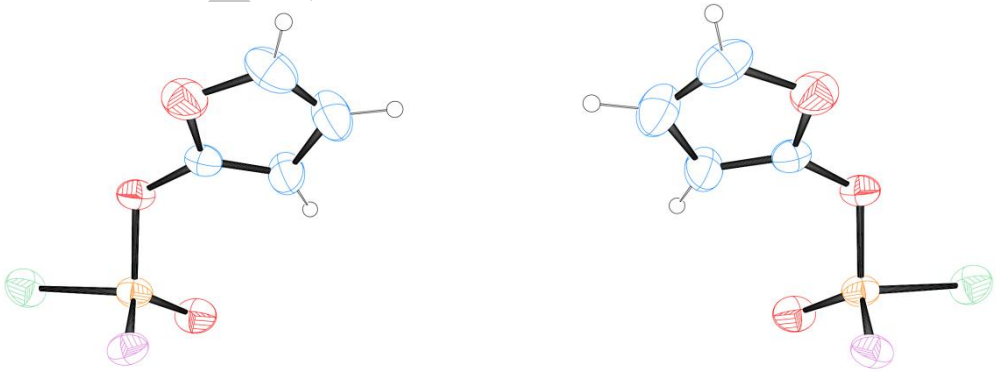

(a) (b)

Fig. 4.

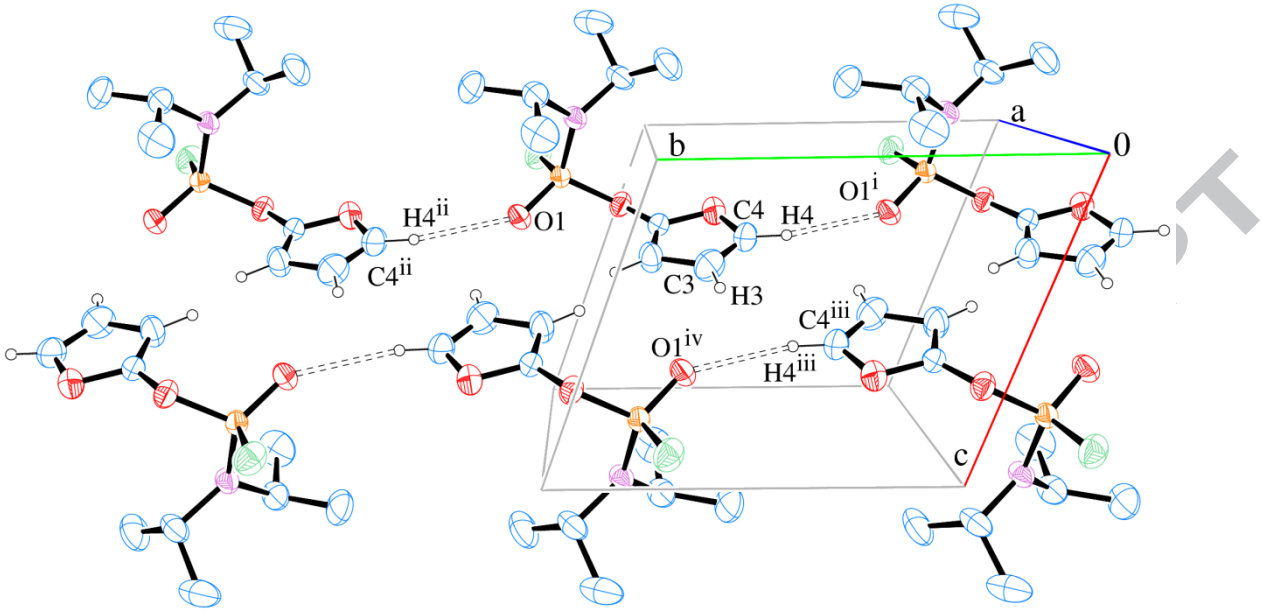

Fig. 5.

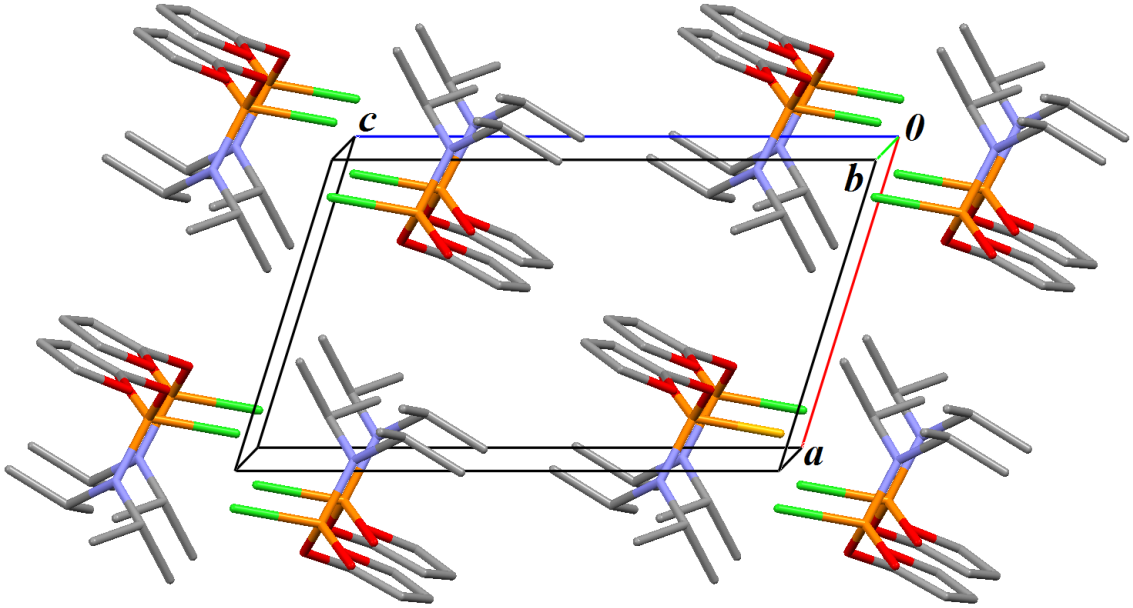

Fig. 6.

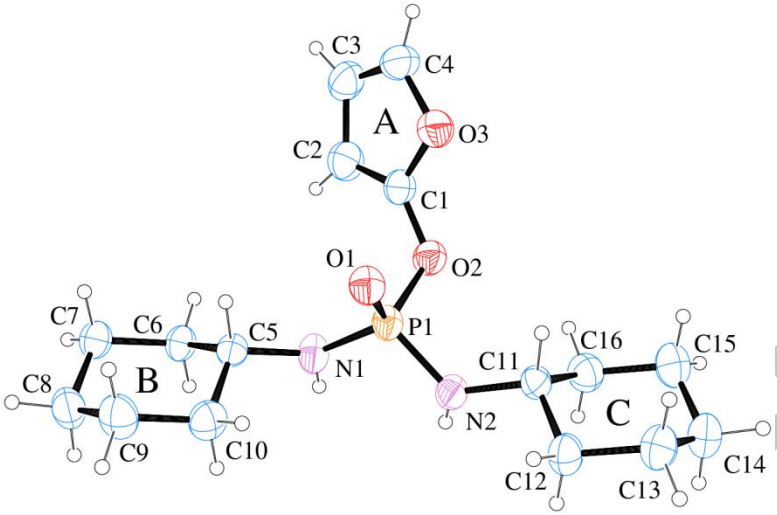

Fig. 7.

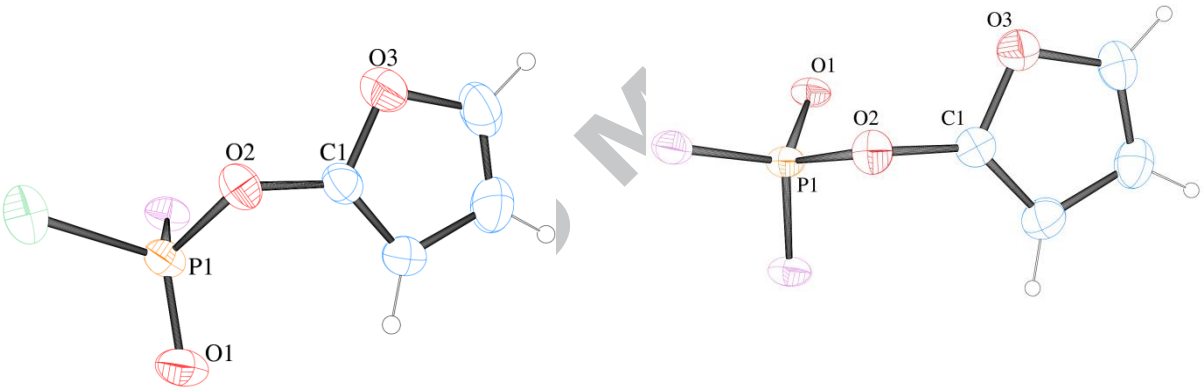

(a) (b)

Fig. 8.

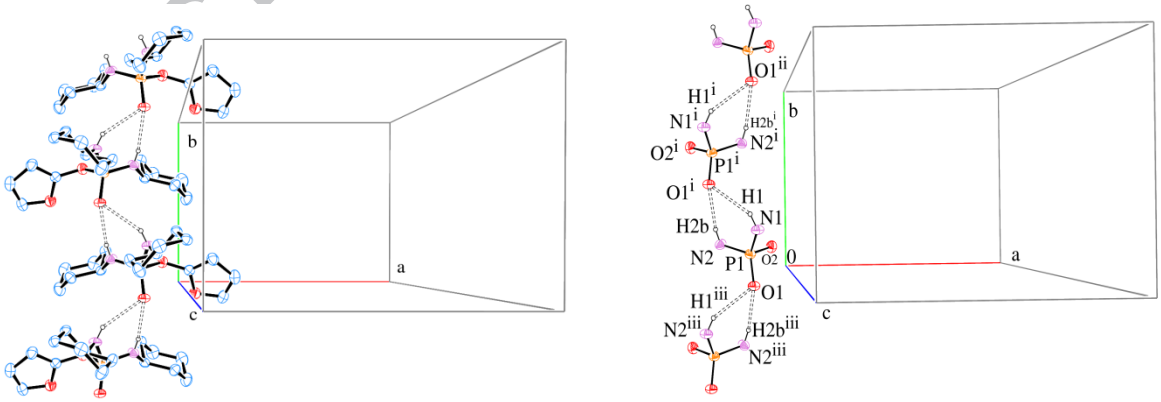

(a) (b)

Fig. 9.

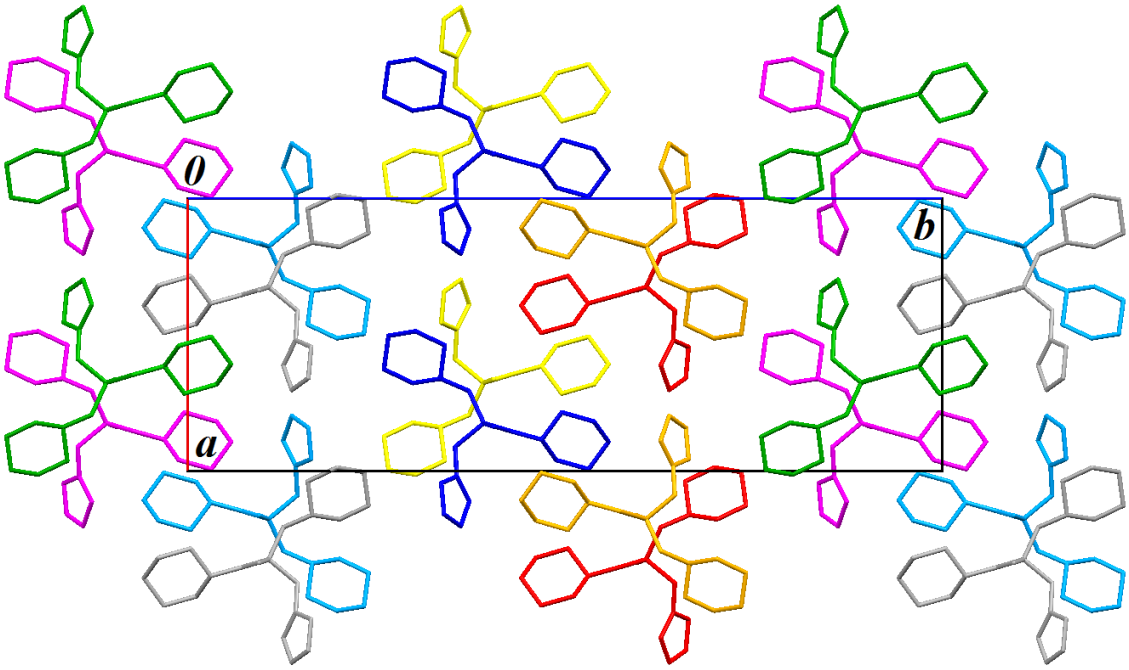

Fig. 10.

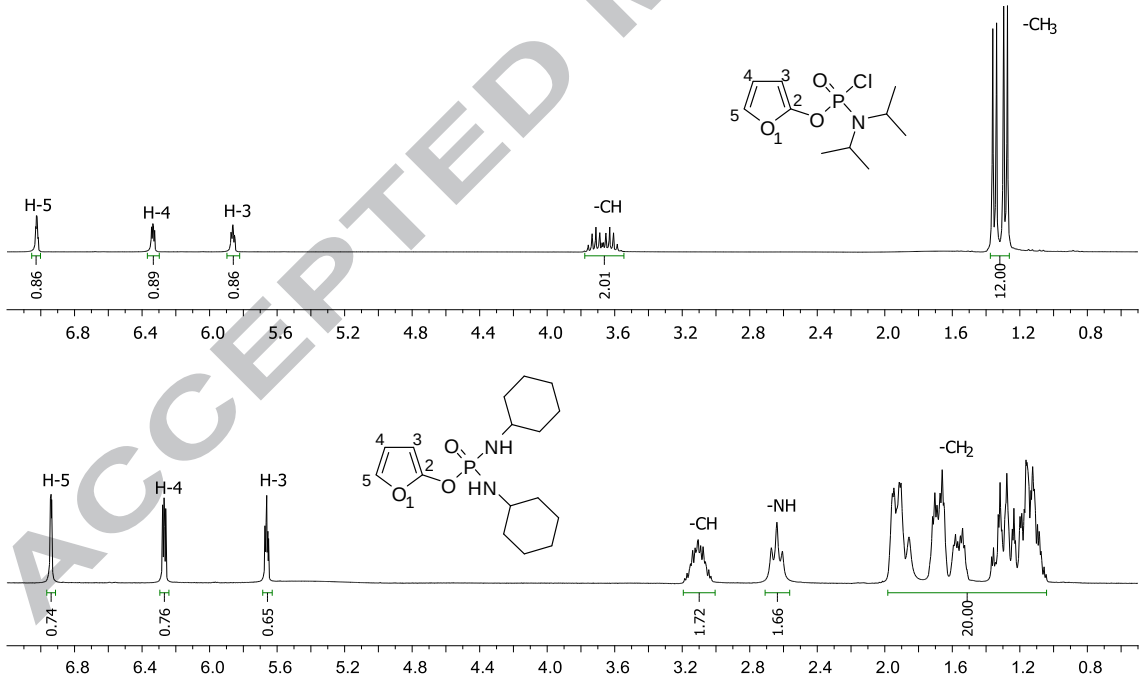

Fig. 11.

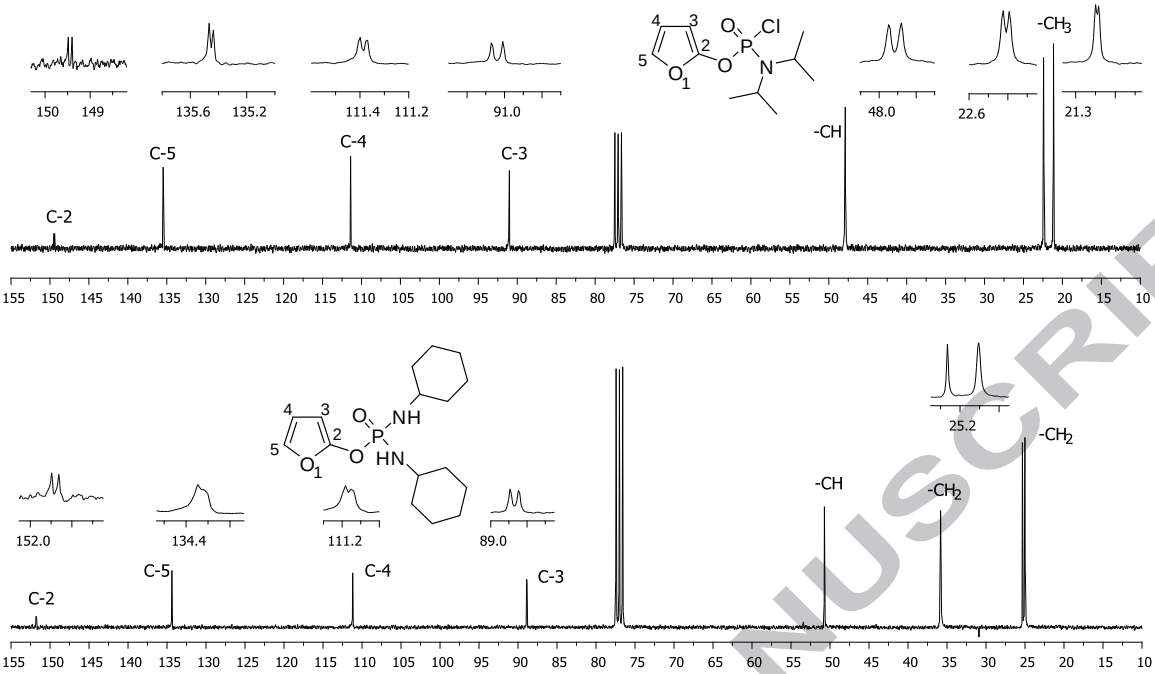

Fig. 12.

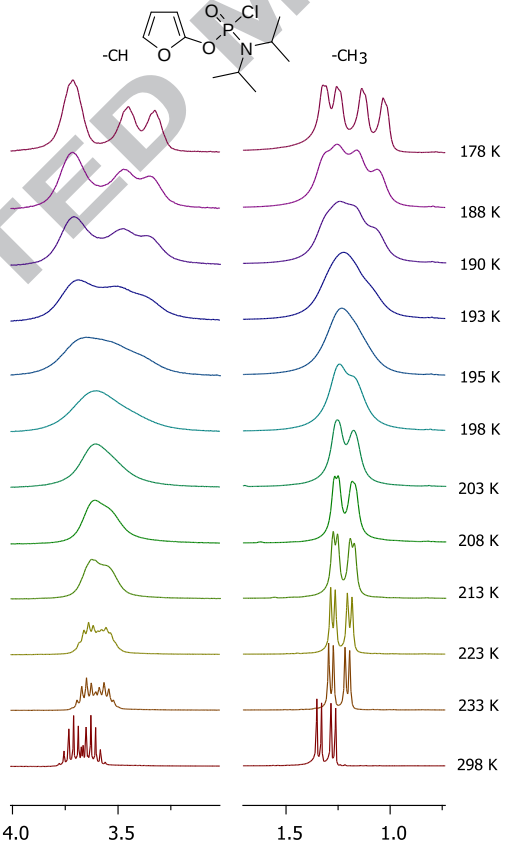

Fig. 13.

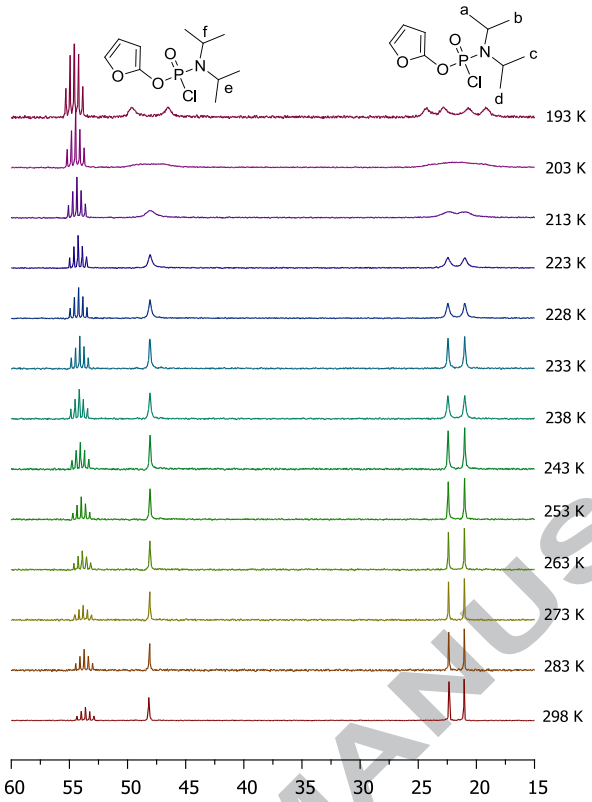

Scheme1.

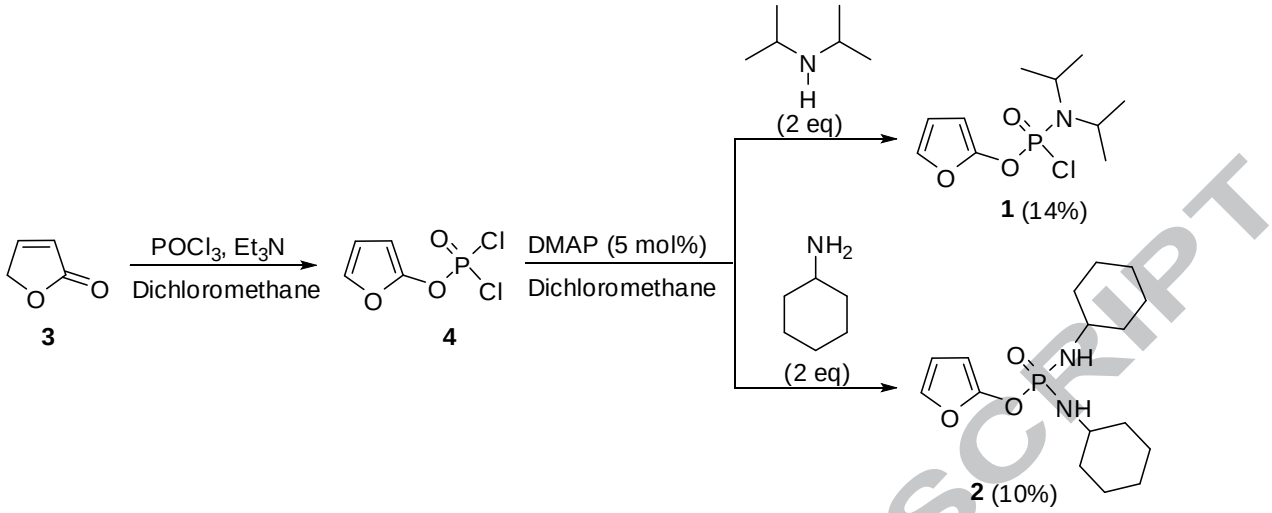

Scheme 2.

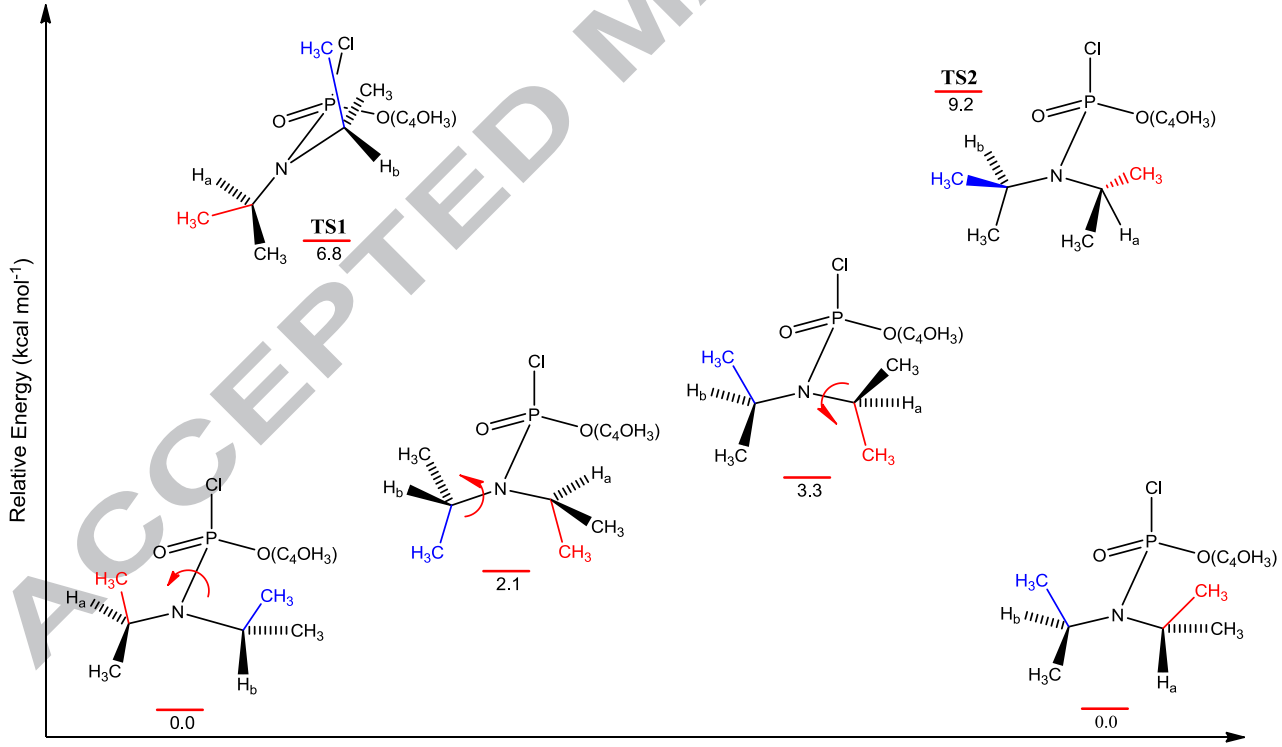

Table 1 - Crystal data, data collection details and structure refinement results for **1** and **2**.

	1	**2**
Empirical formula	$C_{10}H_{17}N_1O_3P_1$	$C_{16}H_{27}N_2O_3P_1$
Formula weight	265.67	326.27
Crystal system	Triclinic	Orthorhombic
Space Group	P-1	Pbca
Unit cell (Å, º)	*a*=7.4216(2) *b*=8.4341(3) *c*=11.9649(4) α=87.914(2) β=73.647(2) γ=70.935(2)	*a*=11.8810(5) *b*=8.9415(3) *c*=32.847(1) α=β=γ=90º
Volume ($Å^3$)	677.94(4)	3489.5(2)
Z	2	8
Density (mg/m^3)	1.301	1.242
μ (mm^{-1})	0.393	0.171
F (000)	280	1408
Crystal size (mm^3)	0.21 x 0.24 x 0.38	0.19 x 0.23 x 0.26
θ_{max} (º)	26	25
Index ranges	-9<=h<=9, -10<=k<=10, -14<=l<=14	-13<=h<=14, -9<=k<=10, -19<=l<=40
Reflections collected	9784	16902
Independent reflections	2681 [R(int) = 0.0741]	3396 [R(int) = 0.0944]
Completeness to θ_{max} (%)	99.1	98.6
Data/restraints/parameters	2681 / 0 / 149	3396 /0/ 205
Goodness-of-fit on F^2	1.048	0.979
Final R índices [I>2σ(I)]	R1 = 0.0462, wR2 = 0.1236	R1 = 0.0477, wR2 = 0.1099
R indices (all data)	R1 = 0.0588, wR2 = 0.1323	R1 = 0.0981, wR2 = 0.1298
$\Delta\rho_{max}$ and $\Delta\rho_{min}$ ($e.Å^{-3}$)	0.390 and -0.315 e.Å-3	0.156 and -0.211

Table 2 - Experimental (X-ray) and calculated selected bond lengths [Å] and angles [°] for **1** and MOGUL [41] bond analysis.

Geometric Parameter	Bond length	Mogul average query	B3LYP/ 6-311++G(2d,p)	Geometric parameter	Bond angle	Mogul average query	B3LYP/ 6-311++G(2d,p)
C10–C8	1.516(4)	1.52(3)	1.536	C2–C3–C4	108.0(3)	107(2)	106.524
C6–C5	1.506(4)	1.52(3)	1.529	O3–C4–C3	109.7(2)	110(2)	110.280
C7–C5	1.528(4)	1.52(3)	1.533	C10–C8–N1	111.9(2)	113(2)	114.579
C9–C8	1.512(4)	1.52(3)	1.531	C6–C5–N1	111.1(2)	113(2)	114.144
C3–C2	1.422(4)	1.42(5)	1.434	C7–C5–N1	112.0(2)	113(2)	112.490
O3–C4	1.406(3)	1.38(3)	1.369	C9–C8–N1	110.8(2)	113(2)	113.037
C3–C4	1.292(4)	1.32(4)	1.354	C8–N1–C5	117.3(2)	118(3)	124.980
C5–N1	1.500(3)	1.49(2)	1.501	O2–P1–O1	114.95(9)	110(4)	115.699
C8–N1	1.490(3)	1.49(2)	1.493	C4–O3–C1	104.2(2)	107(1)	106.292
P1–O2	1.605(1)	1.57(1)	1.640	O3–C1–C2	113.2(2)	109(4)	111.650
P1–Cl1	2.015(1)	2.02(5)	2.071	C3–C2–C1	105.0(2)	108(1)	105.252
O3–C1	1.329(3)	1.35(3)	1.350	P1–N1–C5	121.6(2)	121(3)	116.189
C2–C1	1.311(3)	1.39(4)	1.355	P1–N1–C8	119.9(2)	121(3)	118.680
O2–C1	1.365(3)	1.36(2)	1.358	O2–P1–N1	107.0(1)	104(5)	106.524
P1–N1	1.606(2)	1.62(2)	1.645	O1–P1–N1	116.6(1)	114(2)	115.699
P1–O1	1.452(2)	1.47(3)	1.465	Cl1–P1–N1	109.2(1)	107(2)	107.994
				O2–P1–Cl1	95.12(6)	103(2)	95.664
C10–C8–C9	112.7(3)	112(3)	111.194	O2–C1–C2	131.4(2)	132(3)	132.586
C7–C5–C6	113.2(3)	112(3)	111.977	O1–P1–Cl1	111.8()	109(1)	113.175

Table 3 - Experimental (X-ray) and calculated selected bond lengths [Å] and angles [°] for **2** and MOGUL [41] bond analysis.

Geometric Parameter	Bond length	Mogul average query	B3LYP/ 6-311++G(2d,p)	Geometric parameter	Bond angle	Mogul average query	B3LYP/ 6-311++G(2d,p)
C13–C12	1.528(3)	1.53(3)	1.534	C8–C7–C6	112.0(2)	111(2)	111.787
C14–C13	1.501(4)	1.51(4)	1.533	C8–C9–C10	111.0(2)	111(3)	111.675
C15–C14	1.513(3)	1.51(4)	1.534	C9–C8–C7	110.7(2)	111(4)	111.255
C15–C16	1.520(3)	1.53(3)	1.534	C2–C3–C4	107.1(2)	107(2)	106.842
C7–C6	1.518(3)	1.53(3)	1.534	O3–C4–C3	110.5(2)	110(2)	110.089
C8–C7	1.498(3)	1.51(4)	1.532	C13–C12–C11	111.4(2)	111(2)	111.864
C9–C10	1.510(3)	1.53(3)	1.534	C15–C16–C11	111.6(2)	111(2)	111.747
C9–C8	1.517(3)	1.51(4)	1.533	C7–C6–C5	111.8(2)	111(2)	111.861
C3–C2	1.424(4)	1.42(5)	1.435	C9–C10–C5	112.0(2)	111(2)	111.883
O3–C4	1.371(3)	1.38(3)	1.374	C10–C5–C6	110.6(2)	111(2)	110.945
C3–C4	1.315(4)	1.32(4)	1.353	C12–C11–C16	110.9(2)	111(2)	110.803
C10–C5	1.505(3)	1.51(3)	1.535	C10–C5–N1	112.6(2)	111(2)	111.889
C12–C11	1.515(3)	1.51(3)	1.536	C12–C11–N2	109.6(2)	111(2)	109.983
C16–C11	1.515(3)	1.51(3)	1.535	C16–C11–N2	112.8(2)	111(2)	112.456
C6–C5	1.505(3)	1.51(3)	1.536	C6–C5–N1	111.0(2)	111(2)	110.999
C11–N2	1.471(3)	1.47(2)	1.464	P1–N1–C5	123.2(1)	124(2)	127.827
C5–N1	1.471(3)	1.47(2)	1.472	P1–N2–C11	123.7(1)	124(2)	129.383
P1–O1	1.461(1)	1.48(1)	1.472	O2–P1–O1	108.3(8)	113(2)	116.179
O3–C1	1.346(2)	1.35(3)	1.355	C4–O3–C1	105.7(2)	107(1)	106.196
C2–C1	1.336(3)	1.39(4)	1.355	O3–C1–C2	111.4(2)	109(4)	111.658
O2–C1	1.353(2)	1.36(2)	1.349	C3–C2–C1	105.3(2)	108(1)	105.214
P1–O2	1.640(1)	1.60(1)	1.651	O1–P1–N1	113.63(9)	113(4)	110.529
P1–N1	1.612(2)	1.62(1)	1.656	O1–P1–N2	117.47(9)	113(4)	115.129
P1–N2	1.601(2)	1.62(1)	1.649	O2–P1–N1	107.47(9)	103(5)	104.340
				O2–P1–N2	101.67(9)	103(5)	97.831
C14 C13 C12	111.1(2)	111(2)	111.750	N2–P1–N1	107.3(1)	109(2)	111.768
C14 C15 C16	111.1(2)	111(2)	111.698	O2–C1–C2	133.4(2)	131(3)	133.844
C15 C14 C13	111.3(2)	111(3)	111.193				

Table 4 – Intermolecular hydrogen bond length (Å) and angles (°) for **1**. 'D' and 'A' mean hydrogen donor and acceptor, respectively.

D-H...A	D-H	H...A	D...A	D-H...A
N1-H1...O1^{i}	0.77(3)	2.44(2)	3.110(2)	147(2)
N2-H2b…O1^{i}	0.72(3)	2.22(3)	2.908(2)	162(3)

Symmetry codes (as Fig. 8: $^{(i)}$ -x-1/2, y+1/2, z

Table 5 - Selected coupling constant at 298 K of compounds **1** and **2**.

Compound	$^{4}J_{H3,P}$	$^{5}J_{H4,P}$	$^{5}J_{H5,P}$	$^{3}J_{C3,P}$	$^{4}J_{C4,P}$	$^{4}J_{C5,P}$
1	1.2	0.9	0.9	4.4	2.1	2.2
2	1.2	0.3	0.6	3.5	1.2	1.2

Graphical abstract